Specific Absorption Rates and Magnetic Properties of Ferrofluids with Interaction Effects at Low Concentrations

Ainhoa Urtizberea,[†] Eva Natividad,*,[‡] Ana Arizaga,[†] Miguel Castro,[‡] and Arturo Mediano[§]

Instituto de Ciencia de Materiales de Aragón, CSIC - Universidad de Zaragoza, Sede Campus Plaza San Francisco, Pza. San Francisco s/n, 50009 Zaragoza, Spain, Instituto de Ciencia de Materiales de Aragón, CSIC - Universidad de Zaragoza, Sede Campus Río Ebro, María de Luna, 3, 50018 Zaragoza, Spain, and Grupo de Electrónica de Potencia y Microelectrónica (GEPM), Instituto de Investigación en Ingeniería de Aragón, Universidad de Zaragoza, María de Luna, 3, 50018 Zaragoza, Spain

The specific absorption rate (SAR) of a maghemite-based ferrofluid, measured at 315 K, 3 kA/m, and 109 kHz, was found to double as the ferrofluid concentration was decreased by a factor of 4. The ferrofluid contained nonagglomerated, highly crystalline, and monodisperse nanoparticles with an average size of 11.6 nm and an initial concentration of 8.14 mg/mL. The magnetic characterization of three different concentrations of this ferrofluid revealed several effects typical of the presence of magnetic interactions, such as the decrease of initial susceptibility values (liquid ferrofluid) and Néel relaxation times, τ_N (frozen ferrofluid), with increasing concentration. The accurate SAR determination in adiabatic conditions allowed estimating the τ_N values of the liquid ferrofluid, which displayed the same trend against concentration as those obtained in the frozen state. Such a trend allowed explaining qualitatively the degradation of the heating performance of the ferrofluid upon increasing concentration. Eventually, correlation between τ_N values in both states was discussed in terms of several theoretical models described in the literature and developed to explain the properties of an assembly of nanoparticles with dipolar interactions.

Introduction

The amount of heat released by magnetic nanoparticles (MNPs) subjected to an alternating magnetic field is a key factor for some biomedical applications like magnetic fluid hyperthermia (MFH) for cancer treatment[1] or thermally assisted drug release.[2] In particular, for MFH, the heat generated by the nanoparticles causes a temperature increase of the tissues that may, either modify the conditions in which the cells will develop and grow (hyperthermia[3]), inducing tumor regression and/or cell damage in combination with other toxic agents, or cause direct necrosis (thermoablation) of the cancerous cells, at higher final temperatures. Clinical tests in humans have already been performed, namely, to treat prostate cancer[4] and glioblastoma multiforme.[5]

The heating capacity of MNPs is quantified by the specific absorption rate (SAR), which accounts for the heating power per mass unit of dissipating material. This magnitude depends on the MNP properties,[1,6] such as phase composition, shape, magnetic anisotropy, mean size, and size distribution, and also on the alternating magnetic field parameters, namely, amplitude and frequency. All of these factors determine and influence the heat dissipation mechanisms of the MNPs, and therefore their SAR values.

In MFH, a colloidal suspension containing properly coated MNPs is introduced into the body to reach cancerous tissue. Small particles of the order of tens of nanometers are desired, since they can be better dispersed throughout the tissue and present better body clearance characteristics.[7] For the case of maghemite or magnetite nanoparticles, widely used due to their biocompatibility, these sizes lie well below the critical size of single domain particles.[8] Such particles are likely to lie also in the superparamagnetic regime,[9] in which the heat dissipation is due to the thermal relaxation of magnetic moments.[1] In this situation, it has been demonstrated that monodisperse particles give optimum SAR values, and that the heating power decreases strongly as the standard deviation of the size distribution increases.[10] The Hyeon synthetic method,[11] which allows obtaining highly crystalline and monodisperse nanoparticles of different sizes, is then a suitable synthetic procedure for fabricating superparamagnetic nanoparticles with high theoretical heating powers.

In practice, the spatial arrangement, concentration, and possible agglomeration of the MNPs within the tissues may considerably differ from those of the initial suspensions. Therefore, these are also parameters to take into account when studying the MNP performance, since they can modify their heating ability and, consequently, the heat load to the tumor tissue. In particular, the magnetic nature of the particles may give rise to interparticle interactions. Although the effects of such interactions have been widely studied from the point of view of the MNP magnetic properties, very few works dealing with such effects on the heating ability of MNPs are found in the literature.

In this work, a remarkable decrease of the SAR values with increasing particle concentration is reported for maghemite-based monodisperse MNP suspensions. This behavior has been analyzed and discussed on the basis of the magnetic properties observed. Correlation between SAR data and magnetic properties was attempted in the framework of several theoretical models in the literature developed to explain the magnetic properties of an assembly of interacting particles.

---

 * Corresponding author. Phone: +34 976 762524. Fax: +34 976 761957. E-mail: evanat@unizar.es.
 [†] Instituto de Ciencia de Materiales de Aragón, Sede Campus Plaza San Francisco.
 [‡] Instituto de Ciencia de Materiales de Aragón, Sede Campus Río Ebro.
 [§] Instituto de Investigación en Ingeniería de Aragón.

SARs and Magnetic Properties of Ferrofluids

J. Phys. Chem. C, Vol. 114, No. 11, 2010 **4917**

Experimental Methods

Highly crystalline and monodisperse maghemite nanoparticles were obtained in organic medium by the Hyeon[11] method. This procedure, based on the thermal decomposition of iron pentacarbonyl in the presence of oleic acid, allows varying particle size by controlling the experimental parameters. In our case, a reaction vessel containing 20 mL of octylether and 3.41 g of oleic acid was heated under an argon flush to 100 °C. Then, 0.4 mL of $Fe(CO)_5$ solution was rapidly injected through a septum. Upon injection, the solution turned black in color and bubbled as $Fe(CO)_5$ decomposed. The solution was then heated at 282 °C for 1 h while being vigorously stirred, and finally, the nanoparticle dispersion was cooled to room temperature. The resulting iron nanoparticles were transformed to maghemite by controlled oxidation, using 0.68 g of trimethylamine oxide as a mild oxidant, raising the temperature to 130 °C during a 2 h period and eventually leaving to reflux during a 1 h period. This final ferrofluid was named FF100. Two additional ferrofluids with lower concentrations were prepared by adding octylether to parts of sample FF100. The volume proportions FF100:octylether were 50:50 and 25:75. They were labeled as FF50 and FF25, respectively, related with the decrease in nanoparticle concentration.

The crystalline phase of the nanoparticles was identified by X-ray powder diffraction (XRD). Powder was obtained by washing the ferrofluid with acetone and then leaving dry at room temperature. Patterns were recorded using a D-Max Rigaku diffractometer equipped with a Cu $K_{\alpha1,2}$ radiation source, with 2θ ranging from 5 to 70° at a step size of 0.03°.

Particle size and shape were studied by transmission electron microscopy (TEM) with a Philips CM-30 instrument working at an acceleration voltage of 300 kV. Samples were prepared by putting a drop of the as-prepared maghemite suspension on a carbon-coated copper grid and then left to dry in air.

The dynamic light scattering (DLS) results were obtained using a Zetasizer NanoZS ZEN3600 (Malvern Instruments). The diffusion coefficients were determined from the autocorrelation of the scattered light intensities collected at a 45° scattering angle.

The weight percentage of maghemite in the original fluid was evaluated by thermogravimetric analysis (TGA), using a TGA 5000 apparatus from TA Instruments. About 10 mg of solution was placed in the TGA furnace and heated at a rate of 10 °C/min to 1000 °C in nitrogen atmosphere.

Magnetic measurements were performed using a commercial SQUID magnetometer (Quantum Design-MPMS). The magnetization curves were measured at temperatures of 180 K, 200 K, and room temperature under a maximum magnetic field of 5 T. The diamagnetic contributions of the sample holder and the solvent were subtracted. The dynamic properties from 4.2 K to room temperature were studied through ac susceptibility measurements at frequencies f in the range 1 Hz $\leq f \leq$ 852 Hz by applying an alternating magnetic field amplitude of 4 Oe. Given that such measurements were performed in both the frozen and liquid states of the ferrofluids, we searched to preserve at low temperature the spatial arrangement of the particles in the carrier liquid at room temperature and to avoid aggregates during solid formation. For that purpose, the magnetometer was previously cooled down to a temperature much lower than the freezing point of the solvent ($T_f \sim$ 225 K) under no applied field, so that the arrangement of the particles in the carrier liquid was quenched as the samples were inserted.

The specific absorption rate (SAR) of the three ferrofluids was determined by a calorimetric method using a special-
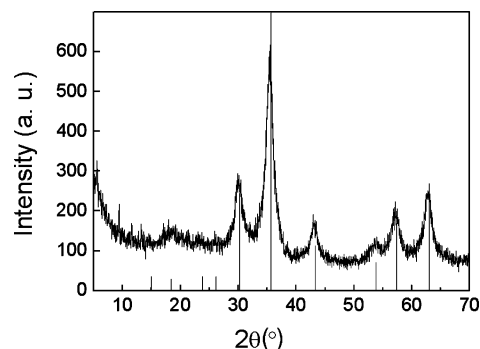
**Figure 1.** XRD patterns of γ-Fe_2O_3 database reference and FF100 powder.

purpose magnetothermal setup[12] working under adiabatic conditions. Direct temperature increments, ΔT, obtained upon application of ac-magnetic-field pulses during a time interval, Δt, were determined. SAR was then calculated as SAR = $(1/m_{NP}) \cdot C \cdot (\Delta T/\Delta t)$, where m_{NP} is the mass of magnetic material and C the heat capacity of the whole sample. Compared to current nonadiabatic installations, this setup and method allow measuring direct sample temperature increments with negligible heat losses, overcoming the limitation of estimating SAR from the temperature-versus-time initial slopes at the onset of the ac magnetic field, where transient effects or heterogeneous sample distributions may derive in appreciable errors in SAR determination.[13]

Measurements were performed on liquid samples at mean temperatures of 315 K. Quartz sample holders sealed with adhesive were used to prevent liquid leakage in the vacuum environment required to achieve adequate adiabatic conditions ($p \leq 10^{-4}$ mbar). The heat capacity of the whole sample (FF + sample holder) was estimated using the mass, concentration, and specific heat capacity of each component. The ac-field amplitude, H_0, and frequency, f, used were 3 kA/m and 109 kHz, respectively, and the final SAR values were obtained by averaging between five and nine heating steps.

Results

The XRD pattern (Figure 1) of the powder obtained from sample FF100 is typical of an inverse spinel structure, meaning the formation of either magnetite (Fe_3O_4) or maghemite (γ-Fe_2O_3). No other relevant peaks apart from those arising from these two phases are observed. Since both phases are very similar in d spacing and reflection intensities, a supporting titration method was used to demonstrate the absence of Fe(II) ions and, consequently, discard the presence of magnetite. Furthermore, the broadening of the most intense peak, the (3 1 1) reflection, was related to the average particle diameter, D, according to Scherrer's formula, $D = 0.9\lambda/\Delta \cos \theta$, where λ is the radiation wavelength (0.154184 nm), Δ is the line broadening measured at half-height, and θ is the Bragg angle. θ and Δ were estimated by fitting the peak to a Lorentzian function with a linear background, from which an average particle diameter of 11.2 nm was obtained.

TEM images (Figure 2) reveal that the ferrofluid particles are quite spherical and uniform in size. The inset shows the particle diameter histogram determined using 360 particles. From the fit to a normal distribution, a particle diameter of 11.6 $\pm$ 1.0 nm was obtained, which reveals a quite monodisperse distribution. Furthermore, the diameter determined by TEM is in good agreement with that calculated from XRD, indicating that nanoparticles are highly crystalline. Figure 2 also suggests
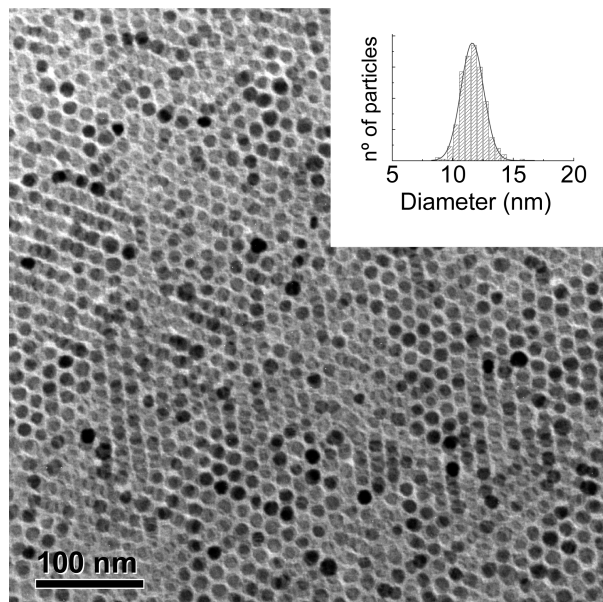
Figure 2. TEM micrograph of sample FF100. Inset: nanoparticle diameter histogram determined from TEM images; continuous line, fit to a normal distribution.
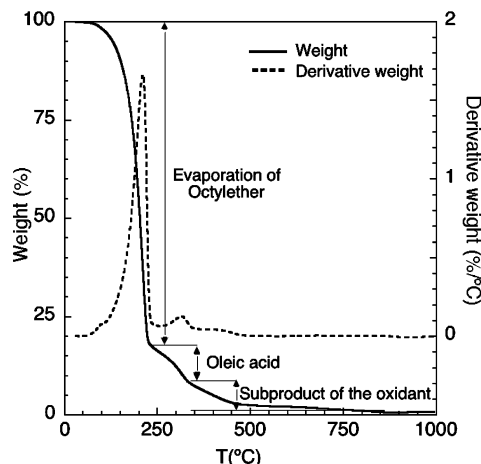
Figure 3. TGA thermogram of sample FF100.

that particles are not aggregated in the ferrofluid, since they present a planar arrangement upon solvent evaporation. The absence of large aggregates at room temperature was also elucidated by using DLS, from which a mean hydrodynamic diameter, D_H, of 14 nm was obtained. This value is slightly higher than D due to the oleic acid layer surrounding the sample, appreciable also in TEM images.

The composition of sample FF100 as obtained from the TGA analysis is in good agreement with the reactant quantities of the synthetic procedure. First, in the temperature range 100−200 °C, the TGA thermogram (see Figure 3) shows a continuous weight loss of about 80%, which corresponds to the evaporation
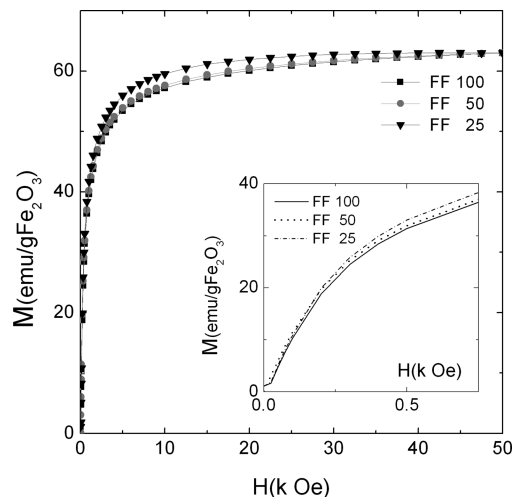
Figure 4. dc magnetization curves at room temperature. Inset: detail susceptibility variation at low fields.

of the octylether (80.6% of the total reactants). The second weight loss of about 10% can be assigned to the oleic acid, which represented 12% of the total reactants. The third weight loss is related to the subproduct of the oxidant, and the residual weight, 0.97%, accounts for the mass of maghemite in the ferrofluid. Since sample FF100 has an experimental mass density of 0.839 g/cm^3, the resulting concentration, c, for FF100 is 8.14 mg of maghemite/mL of ferrofluid.
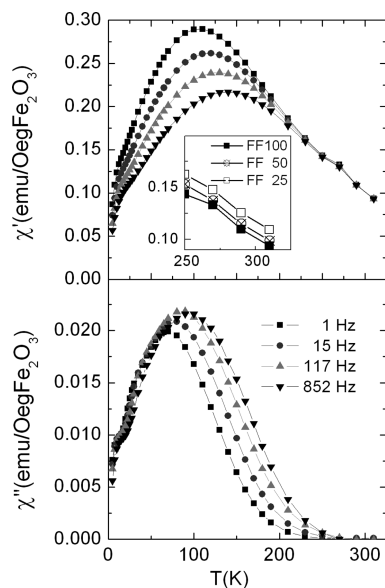
Using the above concentration value, the room-temperature magnetization curve of sample FF100 was scaled to magnetization per unit mass of maghemite (Figure 4), and a saturation magnetization (M_s) value of 63 emu/gFe$_2$O$_3$ (289.80 kA/m in SI units, considering a maghemite mass density of ρ = 4.6 g/cm^3) was obtained. In order to determine the variation of M_s with temperature, the magnetization curves at 180 and 200 K (not shown) were also scaled and a rough fit was performed to these $M_s(T)$ data using the power law $M_s = M_{s(T=0)}(1 - bT^\alpha)$, suitable for nanoparticles.[14] The parameters resulting from the fit are α = 1.7, which gives a Bloch exponent in the range predicted for ultrafine particles (3/2 < α < 3), $b = 1.24 \times 10^{-5}$, and $M_{s(T=0)}$ = 77.3 emu/gFe$_2$O$_3$ (355.58 kA/m), similar to the magnetic saturation value for bulk maghemite. Accordingly, the concentrations of samples FF50 and FF25 were determined relative to that of sample FF100, from their experimental room-temperature magnetization curves (Figure 3), assuming that M_s per unit mass is the same in all samples. The resulting concentrations are c = 4.65 and 1.89 mg/mL for FF50 and FF25, respectively. From these values, volume concentrations were calculated and collected in Table 1.

Considering again Figure 4, differences in approach-to-saturation rates of the room-temperature magnetization curves can be noticed if the three samples are compared. The initial susceptibility is larger for the dilutions than for the original fluid, which responds less readily to the applied field than the dilutions. This fact suggests that, as the ferrofluid concentration increases,

TABLE 1: Nanoparticle Concentration (in mg/mL and % in Volume), Initial Susceptibility at 315 K, Ratio between the Temperature Increment and the Time Interval of Field Application, Heat Capacity and Mass of Nanoparticles of the Samples for SAR Measurements, SAR Values, Effective Relaxation Times, and Néel Relaxation Times Obtained from SAR Measurements for the Three Ferrofluids Considered

sample	c (mg /mL)	c_v (%)	$\chi_{0,315K}$	$\Delta T/\Delta t$ (°C/s)	C (J/°C)	m_{NP} (mg)	SAR (W/g)	τ (s)	τ_N (s)
FF100	8.14	0.18	5.22	6.55×10^{-4}	1.41	2.43	0.38	1.27×10^{-7}	1.32×10^{-7}
FF50	4.65	0.10	5.52	4.94×10^{-4}	1.39	1.47	0.47	1.50×10^{-7}	1.57×10^{-7}
FF25	1.89	0.04	6.12	3.53×10^{-4}	0.43	0.17	0.89	2.61×10^{-7}	2.83×10^{-7}

SARs and Magnetic Properties of Ferrofluids

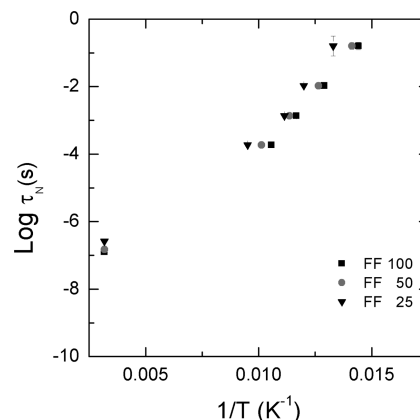*J. Phys. Chem. C, Vol. 114, No. 11, 2010* **4919**

Figure 5. Upper graph: in-phase ac susceptibility for FF100 at various frequencies. Inset: in-phase susceptibility at 1 Hz for samples FF100, FF50, and FF25. Lower graph: out-of-phase ac susceptibility for FF100 at various frequencies.

Figure 6. log τ_N versus $1/T$ for all samples both in the frozen state, calculated from magnetic measurements, and in the liquid state (points at 315 K), as determined from SAR values.

Figure 7. Heating steps at $f = 109$ kHz: experimental data with a smooth fit. The dotted lines are the extrapolation of the T drifts after ac-field application. The double arrowhead lines stand for the $\Delta T \cdot C / m_{NP}$ values.

the alignment of the nanoparticle magnetic moments along the external field gets hindered.

According to their composition, the particle size of the samples is well under the magnetic single-domain/multidomain limit and, also, particles are small enough as to display superparamagnetism at certain temperatures. In this situation, two thermally induced magnetic-moment relaxation mechanisms may occur. These are, Néel relaxation, i.e., reversal of magnetization inside the particle, and Brown relaxation, i.e., rotation of the magnetic particle in the fluid. These mechanisms take place in parallel, with an effective relaxation time expressed as $\tau^{-1} = \tau_N^{-1} + \tau_B^{-1}$. According to ref 10, the out-of-phase component of the ac susceptibility, χ'', can be described by $\chi'' = \chi_0 \omega \tau / (1 + (\omega \tau)^2)$, where $\omega = 2\pi f$ and χ_0 is the equilibrium susceptibility. The average blocking temperature, T_B, which corresponds to the temperature of the maximum of the out-of-phase component, can be defined as the temperature at which the experimental time constant, $\omega^{-1} = (2\pi f)^{-1}$, equals τ. At frequencies, f, fulfilling the condition $(2\pi f)^{-1} > \tau$, thermal relaxation takes place, and if $(2\pi f)^{-1} < \tau$, the magnetic relaxation is blocked because the ac field is changing too fast.

Information about the magnetic dynamics of the three samples was obtained from the temperature dependence of the ac susceptibility at four excitation frequencies. These data are shown in Figure 5 for sample FF100. T_B values were obtained for all samples at four excitation frequencies, and were assigned to their relaxation time values, $\tau = (2\pi f)^{-1}$. Figure 6 shows the log τ versus $1/T$ plot. Given that all T_B values are lower than the melting temperature of the solvent, the ferrofluids at these temperatures are all in the frozen state and, therefore, the particles cannot rotate in the fluid, so that we are regarding information about Néel relaxation times. Then, Figure 6 corresponds to the log τ_N versus $1/T$ plot. It is interesting to note that, for a given T, relaxation is faster as the ferrofluid concentration increases. We have fitted these data using the Néel expression[15] for τ_N, which for a single particle is $\tau_N = \tau_0 \exp(E_b / k_B T)$, where E_b corresponds to the energy barrier for magnetic moment reversal and k_B is the Boltzmann constant. The intercept of the straight lines with the ordinate axis, log τ_0, gives attempt
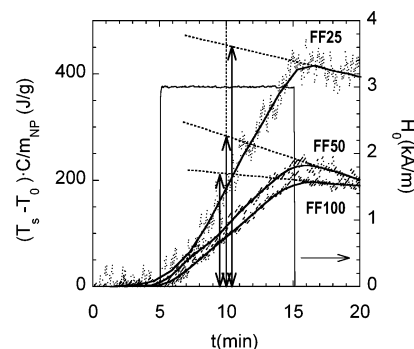
times of the order of 10^{-12} s, lower than the typical τ_0 values for noninteracting particles, between 10^{-8} and 10^{-10} s.[15] The average E_b obtained is 2.35×10^{-20} J, quite alike for the three dilutions within the fit error.

In Figure 5 and above T_B, it is observed that χ'' vanishes at temperatures larger than 275 K, since $\omega \tau \ll 1$. Accordingly, the in-phase susceptibility component, χ', overlaps at all measuring frequencies in this temperature range and equals χ_0, according to $\chi' = \chi_0 / (1 + (\omega \tau)^2)$.[10] This behavior is also observed for the dilutions. Additionally, it should be noticed that χ_0 is larger for the diluted samples (inset in Figure 5) at these temperatures, in accordance with the differences in the approach-to-saturation rates observed for the magnetization curves. In particular, we have calculated the χ_0 values for the three ferrofluids at 315 K (temperature of SAR measurements), through the extrapolation of the χ' trend according to the Curie law. These values, collected in Table 1, are somewhat lower than the value of 6.35 (nondimensional in SI units) calculated from the analytical expression obtained by differentiation of the Langevin equation for low field amplitudes, $\chi_0 \cong (\mu_0 M_s^2 V)/(3k_B T)$, where $M_s = 283.91$ kA/m, as determined from the fit of $M_s(T)$ at $T = 315$ K.

Table 1 also collects the heat capacity and mass of maghemite of the samples used for SAR measurements, together with the SAR values. As an example of this type of measurements, Figure 7 shows three pulses, one for each sample. Due to the low concentration of the samples, we measured ΔT values lower than 1 °C, a fact that explains the slight dispersion of the experimental data. To allow comparison between all samples, the left ordinate axis, in J/g units, was obtained from the sample

temperature, T_s, by subtracting the initial temperature trend, T_0, and by multiplying the result by its C/m_{NP} ratio, to account for the different ratios. The right ordinate axis displays the H_0 trend, to point the field-application interval, with $\Delta t = 600$ s in all cases. Given that the original and diluted ferrofluids come from the same batch, with identical magnetic nanoparticles, SAR values, expressed in watts per gram of magnetic material, should also be similar, and so should the increments in Figure 7. However, these increments are higher for the dilutions, respectively, about 24 and 134% higher, for samples FF50 and FF25. This fact points out a loss of heating power with increasing ferrofluid concentration.

We used for the first time adiabatic SAR measurements to obtain τ_N values in a wider temperature range. Mössbauer spectroscopy,[17] magnetic relaxation, or magnetic noise measurements[18] were used in other works for the same purpose. According to ref 10, SAR in W/g can be expressed as SAR $= \mu_0 \pi f H_0^2 \chi''/\rho$, and therefore, τ values can be estimated for the three ferrofluids through χ'' and using the χ_0 values in Table 1. These values, collected in the same table, reveal that relaxation times decrease with increasing concentration, by a factor of 2 between FF25 and FF100.

However, comparison between relaxation times obtained from magnetic and SAR measurements is not straightforward, since at 315 K the ferrofluids are in the liquid state, nanoparticles are free to rotate within the carrier liquid and the Brownian relaxation mechanism must also be considered. To calculate Brown relaxation time, τ_B, we used the expression $\tau_B = (3V_H\eta)/(k_BT)$,[16] valid for spherical particles, where V_H is the average hydrodynamic particle volume and η the viscosity of the liquid. Considering $\eta = 3.52$ mPa·s for octylether and $V_H = 1.41 \times 10^{-24}$ m³, from the D_H value determined by DLS, a value of 3.43×10^{-6} s is obtained for τ_B. Neglecting the variation of viscosity with ferrofluid concentration, due to the low concentration values, this τ_B value is valid for the three ferrofluids considered. Néel relaxation times can then be deduced and are collected in Table 1. It can be observed that τ_N values are 10 times lower than τ_B, so Néel relaxation is the dominant mechanism, since it occurs much faster. Also, the magnetic moment relaxation is faster as concentration increases, in accordance with the results from the magnetic measurements displayed in Figure 5. The τ_N values determined from SAR measurements were also depicted in Figure 5, related to the measuring temperature, 315 K. It must be noticed that such values, of the order of 10^{-7} s, are much larger than the τ_N value (about 2×10^{-10} s) estimated using the τ_0 and E_b values obtained from magnetic measurements.

The above calculations have been performed assuming that the SAR measuring temperature is higher than T_B at the measuring frequency, that is, that the thermal relaxation mechanisms are not blocked. In this situation, assuming a Néel law for τ_N, and considering a typical value of $\tau_0 = 10^{-9}$ s, we can calculate E_b for the three liquid samples. The estimated energy barriers slightly decrease with concentration, and their mean value, 2.26×10^{-20} J, is not far from that obtained with ac-susceptibility measurements. Using these parameters, we can calculate the T_B value for the three ferrofluids. The resulting T_B value is about 224 K, which is consistent with the assumption that SAR measurements take place well above T_B. Eventually, another rough estimation of the blocking temperature of the samples at 109 kHz can be made considering the Néel expression for τ_N, with $E_b = 2.35 \times 10^{-20}$ J and $\tau_0 = 10^{-12}$ s, as derived from ac measurements, and $\tau_N = (2\pi \cdot f)^{-1} = 1.46 \times$

10^{-6} s. The estimated T_B is 120 K, much lower than the measuring temperature, 315 K.

Discussion

The magnetic properties described above show that the static susceptibility and Néel relaxation time increase with decreasing concentration. In addition, SAR values increase upon dilution, as well as Néel relaxation times obtained from SAR determination. This fact shows that Néel relaxation times obtained at the liquid and frozen states follow the same trend.

The observed concentration effects could be, at first attempt, ascribed to the existence of aggregates in sample FF100, which would have progressively disappeared when diluting the ferrofluid. However, DLS measurements derive a hydrodynamic size for this sample close to that obtained with TEM and discard the existence of large aggregates. Also, due to its low concentration value, sample FF100 is not likely to contain such aggregates. Another possible explanation is the presence of dipolar interactions in the original fluid, which would have become weaker upon dilution. Regarding the effects of interactions on magnetic properties, several pieces of experimental evidence observed here were already reported in the literature for interacting systems: the variation of initial susceptibility in dc magnetization with the increase of the strength of dipolar interactions[19–21] or the small τ_0 values obtained[17] when applying the Néel expression to fit the τ_N values versus $1/T$. However, there are few works dealing with the effects of magnetic interactions on SAR. In ref 22, the SAR of dextran-coated iron-oxide magnetic nanoparticles was reported to be 7 times higher for a tightly associated system with respect to a more loosely associated one. In ref 23, the initial slope of the temperature-versus-time characteristics of ferrofluids based on agglomerated magnetite nanoparticles decreased proportionally to the reduction of the concentration of the ferrofluids, so that no concentration effects were detected.

To our knowledge, our case is the first experimental evidence in which dipolar interactions originate a SAR decrease with increasing concentration. According to the above results, this decrease is related to two effects: (i) The static susceptibility of the nanoparticles decreases with concentration; that is, increasing dipolar interactions make the nanoparticles more stable against field orientation. (ii) Relaxation times decrease with increasing interactions, which causes the particles to relax faster. This affects the heating performance of the sample at a precise excitation frequency. Given that the maximum dissipation by thermal relaxation mechanisms takes place at the optimum frequency $f = (2\pi\tau)^{-1}$, the optimum excitation frequencies should be 610, 1061, and 1253 kHz for samples FF25, FF50, and FF100, respectively, at 315 K. The experimental excitation frequency is then closer to the optimum frequency of the most diluted sample, so dissipation is higher for this sample.

As seen in Figure 6, the τ_N values obtained from SAR reveal the curvature of the log τ_N versus $1/T$ trend at high T, and point that the Néel expression does not describe the variation of τ_N with T. In order to correlate the results obtained in the whole temperature range, we compared our experimental data with some theoretical results about magnetic systems displaying magnetic interactions. The volume concentration of our samples ($c_v \approx 0.18$, 0.10, and 0.04% for FF100, FF50, and FF25, respectively) is very small compared with the concentration of samples well described with models based on spin-glass behaviors,[17,24] characteristics of strong interacting systems. This suggests that such models are not adequate to describe our

system. On the other hand, different models are proposed in the literature to account for systems displaying dipolar interactions. In particular, we considered four models: the Dormann–Bessais–Fiorani model (DBF),[25] the Mørup–Hansen–Tronc model (MHT),[26] the one proposed by P. E. Jönsson, J. L. Garcia-Palacios, M. F. Hansen, and P. Nordblad (JGHN),[27] and the numerical simulation performed by Berkov and Gorn (BG).[28]

The widely used DBF model describes properly the variation of the blocking temperature of an assembly of interacting particles in many experimental cases, except for those related to a collective state. Within this model, relaxation times are described by a Néel law with a modified energy barrier for certain values of the ratio $a_1 M_s^2 V/k_B T$ (in Gaussian units), where $a_1 \approx c_v/\sqrt{2}$. In our case, this ratio is 0.014 and 0.003 for FF100 at 69 and 315 K, respectively. According to DBF, our samples lie in the regime of weak interactions or high T values, in which E_b increases with increasing concentration, and so does τ_N. The trend of our samples is just the opposite for both the frozen and liquid states, so this model seems not to describe our sample behavior.

In the MHT model, the variation of τ_N with the blocking temperature is also described by a Néel law with a modified energy barrier as $\tau_N = \tau_0 \exp[\alpha - (1/3)\beta_{av}^2(1 - 3/4\alpha^{-1})]$, with $\alpha = E_{b0}/k_B T$ and $\beta_{av}^2 = 2[(\mu_0/4\pi)^2 \mu^4 \Sigma d_{nn}^{-6}]/(k_B T)^2$. In these expressions, E_{b0} is the barrier energy for noninteracting particles, μ is the mean magnetic moment, and $\Sigma d_{nn}^{-6} = (\zeta D)^{-6} \Sigma a_{nn}^{-6}$, where ζD is the average interparticle distance $(\zeta^3 D^3 = V/c_v)$ and the estimation of Σa_{nn}^{-6} gives values between 10 and 20, according to MHT. Within this model, the energy barrier decreases with increasing strength of interactions for $\alpha > 1$, which is our case. Using $M_s(T \rightarrow 0) = 356.181$ kA/m, the average particle volume and the c_v value for sample FF100, and $\Sigma a_{nn}^{-6} = 15$, we obtained a β_{av}^2 value of $54.82/T^2$. Fitting magnetic data in Figure 5 to the previous expression, we obtained $\alpha = 1785/T$, that is, $E_{b0} = 2.46 \times 10^{-20}$ J. This implies that the correction to the energy barrier is negligible for our c_v values. For example, at the lowest measured T_B, 69.37 K, the values of α and $(1/3)\beta_{av}^2(1 - 3/4\alpha^{-1})$ for FF100 are 25.73 and 3.69×10^{-3}, respectively. Consequently, our experimental results are not described, since τ_N values scarcely vary within our concentration range.

In the JGHN theoretical approach, the expression for the relaxation time is $\tau_N = \tau_0 e^\sigma \phi$, with ϕ being a function of λ, σ, and ξ_d, where λ is the damping constant, $\xi_d = \mu_0 \mu^2 c_v/4\pi V k_B T$, and $\sigma = E_{b0}/k_B T$. Our c_v values are small enough as to give $\xi_d \ll 1$, so very weak interaction strengths are theoretically expected and our data are susceptible to being described by this model. The thermal variation of the attempt time is taken into account through the expression $\tau_0 = \tau_D \pi^{0.5}/\sigma^{3/2}$, where τ_D is the relaxation of an isotropic spin. Within this model, and for $\lambda = 0.1$ (the typical value assumed for ultrafine particles[29,30]), the blocking temperature decreases for increasing interaction, similarly to our experimental results. We estimated τ_D for this λ value, and we fitted simultaneously the low-T data in Figure 5 with the JGHN expression for τ_N, setting as free parameters E_{b0}, which is common to the three ferrofluids, and the three $\xi_d T$ values, one for each concentration. Again, we used $\mu = M_s \cdot V$, with $M_s = 356.181$ kA/m. The derived $\xi_d T$ values not only are not proportional to c_v in each case but also are about 50 times larger than the calculated ones using the experimental c_v values.

This model gives also an analytical expression for the decrease of the static susceptibility value due to dipolar interactions, $\chi_0 = \mu_0 \mu^2/3k_B T(1 - 1/18\xi_d^2 R)$, where $R = 16.8$ in
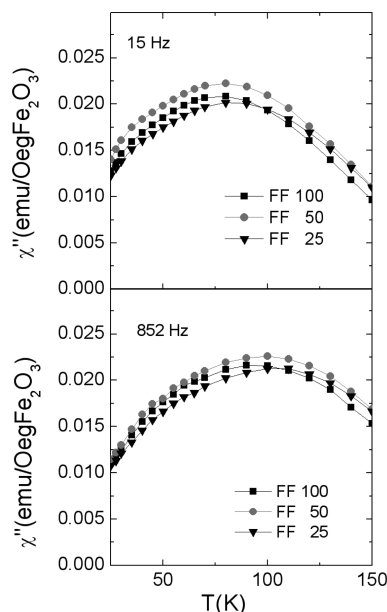
Figure 8. Out-of-phase susceptibility at two frequencies for the three samples.

a simple cubic lattice structure arrangement of particles. We also estimated ξ_d from the experimental χ_0 values at room temperature, and again, the c_v values obtained were about 200 times higher than the real c_v values. Therefore, according to this model, the volume concentrations that would explain our experimental results are much larger than our sample concentrations; that is, the interactions observed experimentally seem much stronger than those corresponding to our sample concentrations.

The previously discussed models offered analytical expressions to calculate the τ_N variation with temperature and concentration of an assembly of particles governed by weak dipolar interactions. The BG model, however, performs a numerical simulation in which no weak-interaction approximations are considered. It provides the temperature dependence of the ac susceptibility for various excitation frequencies and for samples with different particle concentrations, damping parameters, and single-particle anisotropies. With respect to the influence of the interparticle dipolar interaction on χ'', it concludes that the variation with concentration and frequency of both the value and the position of the χ'' maximum depends qualitatively on the single-particle anisotropy and on the damping parameter. Two magnetic anisotropy regimes are distinguished, depending on the value of the factor $\beta = 2K/M_s$ (in Gaussian units): the high- and moderate-anisotropy regime and low-anisotropy case.

We calculated β for our ferrofluids, using an anisotropy constant determined as $K = E_b/V$, the E_b value obtained from the fit of the τ_N low temperature data to the Néel expression, and the saturation magnetization from dc magnetization measurements, 355.6 emu/cm³. The estimated value, $\beta = 4.2 \geq 1$, corresponds to the high- and moderate-anisotropy regime. Within this regime, the theoretical $\chi''(T)$ peak shifts toward lower temperatures with increasing particle concentration, which is the case of our system. Also, the BG model predicts another interesting feature in this regime: χ'' displays a nonmonotonic dependence of the peak height on the particle concentration (displayed for $\beta = 2$ and $\lambda = 0.1$ in ref 28). This effect is also observed in our data (Figure 8): the $\chi''(T)$ peak for sample FF50 is higher that those for samples FF25 and FF100. The effect is small, in accordance with the numerical simulation results.

If we compare the maximum of $\chi''(T)$ for various frequencies, we find that the BG numerical simulation shows a shift of the peak position to higher temperatures as frequency increases for both regimes, which is also in accordance with our results. In addition, it predicts a *decrease* of the peak height as frequency increases for $\beta = 2$ and $\lambda = 0.1$. Here, a discrepancy with our experimental results arises, since the opposite trend is observed. One possible reason for this discrepancy should be that the fixed w parameter used in the simulation ($w = 0.003-0.03$, with $w = \omega/(\gamma \cdot M_s)$ and $\gamma = 2 \times 10^7$ s/Oe) is far from our experimental measuring frequencies.

The above considerations would indicate that our system is in the high- and moderate-anisotropy regime described by the BG model, in which the interparticle dipolar interaction does not fully govern the energy barriers, but such barriers are already created by a relatively high single-particle anisotropy and would decrease with growing interactions. This fact would also be the reason why models based on dipolar interactions as a main contribution to the energy-barrier variations are not applicable to our systems. Therefore, correlation between SAR values and magnetic measurements should be attempted in the framework of the BG numerical simulations, using the specific values of our sample characteristics and measuring conditions.

Conclusions

The specific absorption rate (SAR) and magnetic properties of three ferrofluids (FFs) with different concentrations of the same maghemite nanoparticles have been determined. Particles, obtained by the Hyeon method in organic medium, were nonagglomerated, highly crystalline, and monodisperse, with a mean diameter of 11.6 nm. Furthermore, at the temperature and ac-field frequency characterization ranges, they behaved as superparamagnetic, displaying thermally induced magnetic-moment relaxation phenomena.

Despite the low concentration values of the three FFs, both SAR and magnetic properties displayed magnetic interaction effects. The initial susceptibility in static magnetization measurements was larger for the most diluted sample, indicating that the most concentrated sample responded less readily to the applied field. From ac magnetic measurements, the blocking temperature, T_B, determined at a given frequency increased with decreasing FF concentration. From the log τ_N versus $1/T$ plot, it was concluded that, for a given T, Néel relaxation got faster as the FF concentration increased, and that the fitting of these data to the Néel equation gave τ_0 values 10^3 times lower than the typical τ_0 values for noninteracting particles.

SAR determination of the liquid samples at room temperature pointed out a loss of heating power with increasing FF concentration. The accurate determination of this magnitude under adiabatic conditions allowed using for the first time this kind of measurements to calculate τ_N values in a wider temperature range. This relaxation time as obtained from SAR results was found to decrease with increasing concentration, pointing that τ_N obtained at the liquid and frozen states followed the same trend. The decrease of τ_N originated an increase of the optimum excitation frequency for maximum heat dissipation, and a worse heating performance at 109 kHz for more concentrated samples.

Correlation between τ_N values obtained at liquid and frozen states was attempted in the framework of different models proposed in the literature to account for systems displaying dipolar interactions. All models giving a dominant role to dipolar interparticle interactions were unable to describe our results, since they predicted either opposite trends or smaller interaction effects for our concentration values. The BG numerical model (Berkov and Gorn) explained qualitatively most of the trends observed in our $\chi''(T)$ measurements within the high- and moderate-magnetic anisotropy regime, in which the single-particle anisotropy would create the energy barriers and interparticle dipolar interaction would decrease them. However, further simulation results would be necessary to successfully correlate SAR values and magnetic measurements.

References and Notes

(1) Hergt R.; Andrä W. *Magnetism in Medicine*, 2nd ed.; Wiley-VCH: Weinheim, Germany, 2007; p 550.
(2) Brazel, C. S. *Pharm. Res.* **2009**, *26*, 644.
(3) Gazeau F.; Levy M.; Wilhelm C. *Nanomedicine* **2008**, *3*, 831.
(4) Johannsen, M.; Gneveckow, U.; Eckelt, L.; Feussner, A.; Waldofner, N.; Scholz, R.; Deger, S.; Wust, P.; Loening, S. A.; Jordan, A. *Int. J. Hyperthermia* **2005**, *21*, 637.
(5) Maier-Hauff, K.; Rothe, R.; Scholz, R.; Gneveckow, U.; Wust, P.; Thiesen, B.; Feussner, A.; von Deimling, A.; Waldoefner, N.; Felix, R.; Jordan, A. *J. Neuro-Oncol.* **2007**, *82*, 53.
(6) Hergt, R.; Dutz, S.; Roder, M. *J. Phys.: Condens. Matter* **2008**, *20*, 385214.
(7) Choi, H. S.; Liu, W.; Misra, P.; Tanaka, E.; Zimmer, J. P.; Ipe, B. I.; Bawendi, M. G.; Frangioni, J. V. *Nat. Biotechnol.* **2007**, *25*, 1165.
(8) Fabian, K.; Kirchner, A.; Williams, W.; Heider, F.; Leibl, T.; Hubert, A. *Geophys. J. Int.* **1996**, *124*, 89.
(9) Muxworthy, A. R.; Dunlop, D. J.; Williams, W. *J. Geophys. Res., [Solid Earth]* **2003**, *108*, 2281.
(10) Rosensweig, R. E. *J. Magn. Magn. Mater.* **2002**, *252*, 370.
(11) Hyeon, T.; Lee, S. S.; Park, J.; Chung, Y.; Bin Na, H. *J. Am. Chem. Soc.* **2001**, *123*, 12798.
(12) Natividad, E.; Castro, M.; Mediano, A. *Appl. Phys. Lett.* **2008**, *92*, 093116.
(13) Natividad, E.; Castro, M.; Mediano, A. *J. Magn. Magn. Mater.* **2009**, *321*, 1497.
(14) Hendriksen, P. V.; Linderoth, S.; Lindgard, P. A. *Phys. Rev. B* **1993**, *48*, 7259.
(15) Neel, L. *C. R. Hebd. Seances Acad. Sci.* **1949**, *228*, 664.
(16) Brown, W. F. *Phys. Rev.* **1963**, *130* (5), 1677.
(17) Dormann, J. L.; Fiorani, D.; Tronc, E. *J. Magn. Magn. Mater.* **1999**, *202*, 251.
(18) Jönsson, T.; Nordblad, P.; Svedlindh, P. *Phys. Rev. B* **1998**, *57*, 497.
(19) Kachkachi, H.; Azeggagh, M. *Eur. Phys. J. B* **2005**, *44*, 299.
(20) Skumiel, A.; Józefczak, A.; Hornowski, T.; Ašbowski, M. *J. Phys. D: Appl. Phys.* **2003**, *36*, 3120.
(21) Vargas, J. M.; Nunes, W. C.; Socolovsky, L. M.; Knobel, M.; Zanchet, D. *Phys. Rev. B* **2005**, *72*, 184428.
(22) Dennis, C. L.; Jackson, A. J.; Borchers, J. A.; Ivkov, R.; Foreman, A. R.; Lau, J. W.; Goernitz, E.; Gruettner, C. *J. Appl. Phys.* **2008**, *103*, 07A319.
(23) Eggeman, A. S.; Majetich, S.; Farrell, D.; Pankhurst, Q. A. *IEEE Trans. Magn.* **2007**, *43*, 2451.
(24) Jönsson, P. E. *Adv. Chem. Phys.* **2004**, *128*, 191.
(25) Dormann, J. L.; Bessais, L.; Fiorani, D. *J. Phys. C: Solid State Phys.* **1988**, *21*, 2015.
(26) Hansen, M. F.; Mørup, S. *J. Magn. Magn. Mater.* **1998**, *184*, 262.
(27) Jönsson, P. E.; García-Palacios, J. L.; Hansen, M. F.; Nordbald, P. *J. Mol. Liq.* **2004**, *114*, 131.
(28) Berkov, D. V.; Gorn, N. L. *J. Phys.: Condens. Matter* **2001**, *13*, 9369.
(29) Dormann, J. L.; D'Orazio, F.; Lucari, F.; Tronc, E.; Prené, P.; Jolivet, J. P.; Fiorani, D.; Cherkaoui, R.; Noguès, M. *Phys. Rev. B* **1996**, *53*, 14291.
(30) Coffey, W. T.; Crothers, D. S. F.; Dormann, J. L.; Kalmykov, Y. P.; Kennedy, E. C.; Wernsdorfer, W. *Phys. Rev. Lett.* **1998**, *80*, 5655.